Ultra-low resistance ohmic contacts to GaN with high Si doping concentrations grown by molecular beam epitaxy

Faiza Afroz Faria,[a] Jia Guo, Pei Zhao, Guowang Li, Prem Kumar Kandaswamy, Mark Wistey, Huili (Grace) Xing, and Debdeep Jena
Department of Electrical Engineering, University of Notre Dame, Indiana 46556, USA

Ti/Al/Ni/Au ohmic contacts were formed on heavily doped n^+ metal-polar GaN samples with various Si doping concentrations grown by molecular beam epitaxy. The contact resistivity (R_C) and sheet resistance (R_{sh}) as a function of corresponding GaN free carrier concentration (n) were measured. Very low R_C values ($<0.09\,\Omega\,mm$) were obtained, with a minimum R_C of $0.035\,\Omega\,mm$ on a sample with a room temperature carrier concentration of $\sim 5 \times 10^{19}\,cm^{-3}$. Based on the systematic study, the role of R_C and R_{sh} is discussed in the context of regrown n^+ GaN ohmic contacts for GaN based high electron mobility transistors. © 2012 American Institute of Physics. [http://dx.doi.org/10.1063/1.4738768]

Wide bandgap, high breakdown voltage, high electron saturation velocity, and high thermal conductivity are properties that make GaN attractive for high temperature, high power, and high frequency electronic device applications. GaN based high-electron-mobility transistors (HEMTs) have been studied extensively, and excellent performance has been demonstrated.[1–7] Further improvement, such as operation at higher frequencies and higher efficiency, requires low resistance ohmic contacts ($R_C < 0.1\,\Omega\,mm$) since it usually dominates the total parasitic resistance. The challenge in forming ohmic contacts to GaN stems from its large bandgap and large Schottky barrier height to most metals. Various methods have been applied to fabricate low-resistance ohmic contacts to GaN.[8–11] Out of these, the lowest contact resistivity values reported so far are $<0.08\,\Omega\,mm$ (Ref. 7) for Ga polar GaN and $<0.027\,\Omega\,mm$ (Ref. 6) for N-polar GaN employing molecular beam epitaxy (MBE) regrown n^+ GaN and graded InGaN with InN cap, respectively. However, a systematic study of the contact resistivity and sheet resistance of the regrown regions is still missing, and constitutes the main aim of this work. Here we systematically investigate annealed Ti/Al/Ni/Au ohmic contacts formed on MBE grown heavily doped n^+ GaN samples by varying the Si doping concentration. The goal is to relate the R_C and R_{sh} to the free carrier concentration (n) in the heavily doped GaN layers. The implication of these findings on design of low-parasitic resistance GaN HEMTs is also discussed.

A series of $\sim 200\,nm$ thick n^+ GaN films were grown using MBE with a rf-plasma nitrogen source. Semi-insulating GaN on SiC templates grown by metal organic chemical vapor deposition (MOCVD) were chosen as substrates. The templates were thoroughly cleaned in organic solvents using ultrasonication, introduced into the loadlock chamber of the MBE system, and outgassed at $200\,°C$. They were then transferred into a buffer chamber and outgassed further at $450\,°C$ for $1.5\,h$. The growth was performed under slightly Ga-rich condition with a low growth rate of $\sim 100\,nm/h$. The growth temperature as measured by a ther-

mocouple was $660\,°C$. Samples labeled A, B, C, and D were grown using Si cell temperatures of 1250, 1280, 1300, and $1320\,°C$, respectively. Atomic force microscopy (AFM) was used to measure the surface roughness of the grown films. Hall-effect measurements were performed to measure the electronic transport properties of the samples. Transmission line measurement (TLM) structures were then fabricated by contact lithography followed by a $1\,min$ descum in oxygen plasma at low power ($125\,W$). The samples were then dipped in HCl:deionized water (1:1) solution for $20\,s$ and rinsed in deionized water for $30\,s$ to get rid of native oxides remaining on the surface before ohmic metal deposition. Ti/Al/Ni/Au ($15/120/40/50\,nm$) stacks were deposited by electron beam evaporation to form the metal contacts. The TLM pads were then etched into mesas using reactive ion etch (RIE) with a mixture of BCl_3, Cl_2 and Ar gas for isolation. A rapid thermal annealing was performed at $840\,°C$ for $15\,s$ under nitrogen environment with a flow rate of $5\,cm^3$ per minute at STP (SCCM). The fabricated TLM structures were then measured using the four-point probe technique. A control sample consisting n^+ GaN ($\sim 50\,nm$)/undoped GaN ($\sim 50\,nm$) layers was grown by MBE where the Si doping in the successive n^+ GaN layers was varied using the same cell temperatures used for the series of four n^+ GaN samples. Secondary ion mass spectrometry (SIMS) was carried out on this control sample to determine the concentration of Si doping in the individual layers.

Low-resistance ohmic contacts involve tunneling and thermionic emission of the electrons across the metal-semiconductor interface. A narrow tunneling barrier and low contact resistance is facilitated by high doping since the depletion depth is inversely proportional to the square root of the doping density. An Arrhenius plot of the Si concentration obtained from the SIMS calibration sample is shown in Fig. 1. Here A, B, C, D refer to Si cell temperatures same as those used for the four n^+ GaN films. The inset of Fig. 1 shows the SIMS profile for Si and O concentrations. The data show the Si doping concentration is very high, ranging from $\sim 1.7 \times 10^{19}$ to $\sim 9.4 \times 10^{19}\,cm^{-3}$. This level of doping makes the n^+ GaN films degenerate, i.e., the Fermi level in

[a]Electronic mail: ffaria@nd.edu.
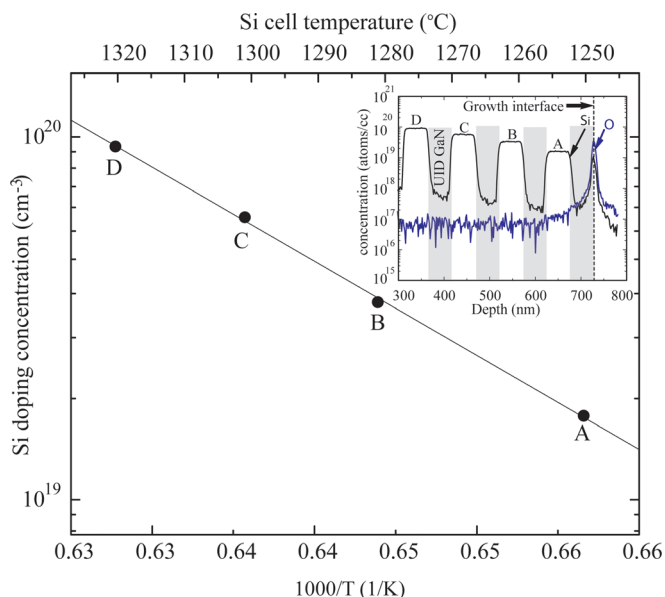
FIG. 1. Arrhenius plot of the Si concentration determined by SIMS, and the SIMS profile for Si and O concentration as a function of depth along growth direction is shown in the inset.

the bulk n^+ GaN is inside the conduction band. The activation energy of Si effusion from the Knudsen cell extracted from this plot is ~ 5.15 eV, in good agreement with the expected value.[12] In Fig. 1 inset, an increased concentration of Si and O can be observed at the growth interface between substrate and epilayer, possibly due to interfacial defects and impurities on substrate surface, an observation that has been widely reported earlier.[13–17] Special care was taken in the study to avoid any spurious conclusions from the high oxygen concentration at the growth interface; the heavily Si doped regions were far thicker than the relatively thin oxygen doped layer, and its effect on the study can safely be neglected.

The background oxygen doping, in addition to the intentional Si dopants of the n^+ GaN films, can contribute to the carrier transport depending on the fraction that is ionized. From Hall-effect measurement data shown in Fig. 2, we conclude a minor contribution ($\sim 10\%$ at most) from the background dopants. The Hall-effect data represent the trend of
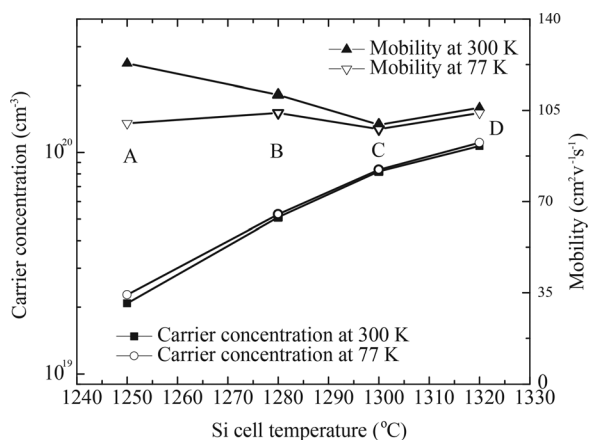
carrier concentration and electron mobility in the n^+ GaN films as a function of corresponding change in doping concentration reflected by the Si cell temperature. Both room temperature (300 K) and 77 K data show that n increases with increasing Si doping. The electron mobility remains fairly constant, indicating again the degenerate carrier distribution. In degenerately doped semiconductors, the mobile electron concentration and the mobility are weak functions of temperature since they are effectively metallic, as shown in Fig. 2. An interesting observation from these measurements is the increase of carrier concentration and decrease in mobility as the Hall-effect measurement temperature is changed from room temperature to 77 K. Similar phenomena were reported by Kim *et al.*[18] for Si doped zinc blende GaN. They attributed this behavior to simultaneous conduction in the conduction band, and in an impurity band associated with the heavy Si doping. According to their explanation, the conduction in high mobility conduction band dominates from room temperature down to around 70 K and below this temperature low mobility conduction via impurity band states dominates. Our observation supports similar mechanism for heavily Si doped wurtzite GaN.

Fig. 3 shows the measured resistivity versus gap spacing plots obtained from room temperature TLM measurements on the n^+ GaN samples using the four-point probe technique. For all 4 samples, R_{sh} and R_C are extracted from the slope and the y-axis (resistivity) intercept of their corresponding linear fits, respectively, as shown in Fig. 3. Fig. 4 shows the R_{sh} values obtained from room temperature and 77 K Hall-effect measurements of the samples compared to those extracted from the TLM measurement. They are in good agreement. The sheet resistance decreases with increasing carrier concentration, as expected. We note that the net sheet resistances of the heavily doped 200 nm n^+ GaN layers are ~ 30–120 $\Omega/\square$. These values are much lower than the 2DEG sheet resistance of typical GaN HEMTs, which ranges from ~ 150–300 $\Omega/\square$. To find the dependence of the contact resistivity on the carrier concentration in the n^+ GaN films, R_C

FIG. 2. Plot of carrier concentration and mobility of the n^+ GaN samples obtained from Hall-effect measurements at room temperature (300 K) and 77 K as a function of corresponding Si cell temperature.
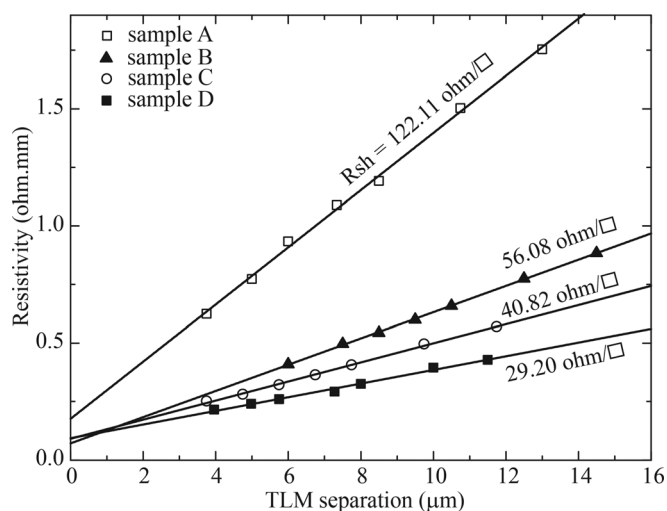
FIG. 3. Measured resistivity versus gap spacing plots obtained from TLM structures measured on samples grown using Si cell temperature of 1250 °C (A), 1280 °C (B), 1300 °C (C), and 1320 °C (D). The solid lines indicate linear fit to the experimental data points and extracted sheet resistance values are indicated for each sample.
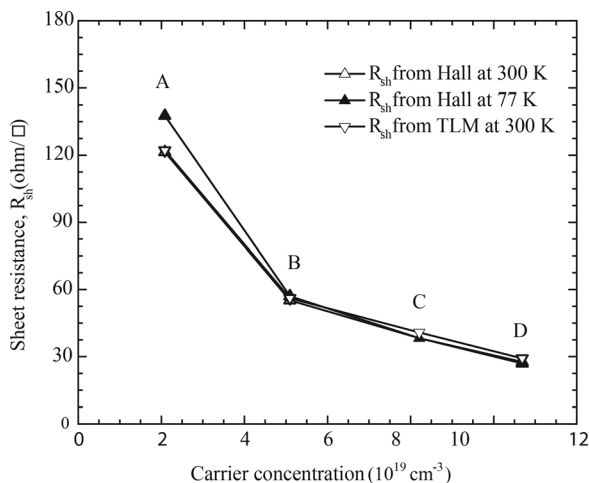
FIG. 4. sheet resistance versus carrier concentration plots obtained from room temperature TLM measurements and Hall measurements at room temperature (300 K) and 77 K.

values are plotted against their room temperature carrier concentration values in Fig. 5. Interestingly, R_C decreases from sample A to B, then increases from B to C and stays reasonably constant below $0.05\,\Omega\,mm$ for samples with higher carrier concentrations. A minimum R_C of $0.035\,\Omega\,mm$ is obtained for sample B, which has a carrier concentration of $\sim 5 \times 10^{19}\,cm^{-3}$. Adopting the TLM error analysis method described by Ueng *et al.*,[20] all extracted R_C values are found to have an error less than 30%. The $2\,\mu m \times 2\,\mu m$ AFM scan of sample B as-grown surface is shown in the inset of Fig. 5. The RMS roughness of $\sim 0.2\,nm$ indicates very smooth surface morphology. Similar AFM scans on all four n^+ GaN samples showed very smooth surfaces with RMS roughness values less than 1 nm. We note that unlike the case of heavy Si-doped GaN by MOCVD growth where degradation of surface and crystal structure is typically observed,[21] MBE growth allows a smooth surface morphology. The smooth morphology also indicates that the surface roughness of as-grown samples is not the main cause of the different contact
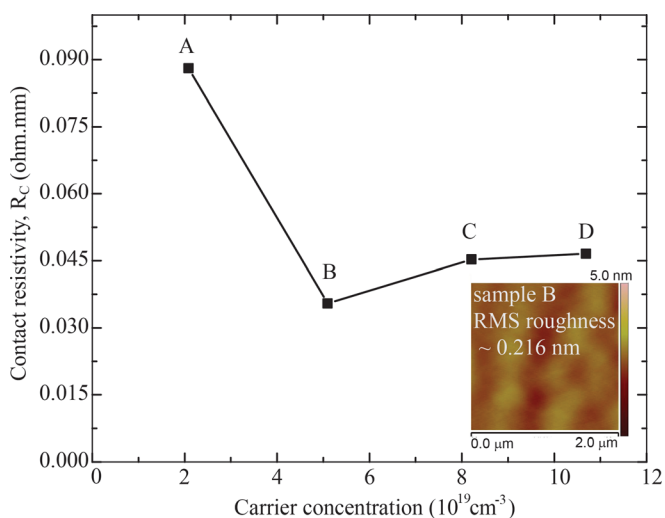
resistances. We observe that the effect of the carrier concentration is more pronounced on the sheet resistance than on the contact resistivity for n^+ GaN samples under such extremely high doping ($>10^{19}\,cm^{-3}$).

We now discuss the roles of R_{sh} and R_C in the context of GaN based HEMTs where regrown n^+ GaN ohmic contacts have proven to be very useful in boosting device performance by lowering parasitic losses. If we consider a typical InAlN/AlN/GaN HEMT structure as shown in the inset of Fig. 6, the total contact resistivity (R_{total}) measured for the HEMT can be divided into three components: R_1, the resistivity between the ohmic metal and regrown n^+ GaN; R_2, resistivity of the n^+ GaN access region; and R_3, resistivity between regrown n^+ GaN and the 2DEG channel. Based on our current study, we can predict how R_1 and R_2 change depending on the amount of doping in the regrown n^+ GaN of such HEMT structures, while R_3 has been investigated in another work.[19] We consider four different cases of HEMTs with n^+ GaN regrown for source drain ohmics using growth conditions similar to those of the four n^+ GaN films studied here. Then $R_1 = R_C$, $R_2 = R_{sh} \times L$, where the distance L (inset of Fig. 6) depends on the alignment of the source, drain metal pads to the regrown regions. So, $R_1 + R_2 = R_C + R_{sh} \times L$.

In Fig. 6, values of $R_1 + R_2$ are plotted using R_C and R_{sh} values of sample A, B, C, and D as a function of their corresponding carrier concentrations. We have chosen 4 typical values of L ranging from 0.2 to $2\,\mu m$. There is a clear trend in change of $R_1 + R_2$ depending on the size of L for heavily doped samples with carrier concentration $>5 \times 10^{19}\,cm^{-3}$ (sample B, C, and D). We may draw some interesting conclusions for GaN based HEMTs with regrown n^+ GaN ohmics based on this observation. Only for structures fabricated with large L ($>0.5\,\mu m$), the change in $R_1 + R_2$ with respect to doping concentration will be dominated by R_{sh}. On the contrary, structures with small L ($<0.5\,\mu m$) will force $R_1 + R_2$ to follow the trend of R_C in terms of change with

FIG. 5. Plot of contact resistivity versus room temperature carrier concentration of sample A, B, C and D. $2\,\mu m$ by $2\,\mu m$ AFM image of sample B with a smooth surface (rms roughness $\sim 0.216\,nm$) is shown in the inset.
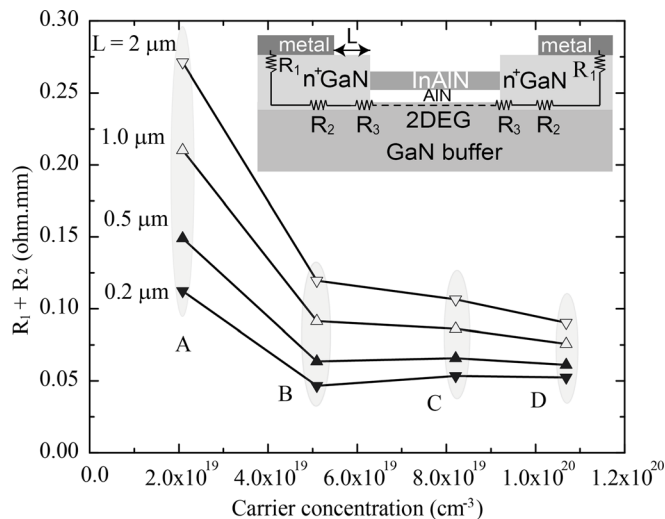
FIG. 6. Calculated values of $R_1 + R_2$ as a function of carrier concentration for regrown n^+ GaN ohmic contacts of a typical HEMT structure (inset). Four different cases of regrown n^+ GaN similar to sample A, B, C, and D have been considered; for each case of regrown n^+ GaN, L is chosen to have 4 different values of 0.2, 0.5, 1, and $2\,\mu m$.

respect to doping concentration. As a result, pushing any further to increase the doping concentration even higher than achieved here in the regrown n^+GaN will not contribute to lower the total contact resistivity of HEMTs employing such regrown contacts.

In summary, alloyed ohmic contacts were fabricated on a series of heavily doped 200 nm n^+GaN samples. The very low sheet resistance values achieved ($\sim$30 $\Omega/\square$) and the ultra-low contact resistivities ($\sim$0.04 Ω mm) are most attractive for integration in GaN HEMTs. Though further studies are required to investigate the solubility limit of Si dopants in GaN grown by MBE, for doping densities approaching $\sim$10^{20}/cm^3, the surface retains a smooth morphology. Further reduction in R_{sh} may be possible if Si doping densities in the n^+GaN films can be pushed to the solubility limit. A comparison of typical HEMT structures also show that the doping densities achieved are high enough so that improvements in HEMT device performance can be more effectively achieved by geometrical alignment than by heavier doping.

[1]Y.-F. Wu, A. Saxler, M. Moore, R.P. Smith, S. Sheppard, P. M. Chavarkar, T. Wisleder, U. K. Mishra, and P. Parikh, IEEE Electron Device Lett. **25**(3), 117–119 (2004).

[2]H. Sun, A. R. Alt, H. Benedickter, E. Feltin, J.-F. Carlin, M. Gonschorek, N. Grandjean, and C. R. Bolognesi, IEEE Electron Device Lett. **31**(9), 957–959 (2010).

[3]R. Wang, P. Sanier, X. Xing, C. Lian, X. Gao, S. Guo, G. Snider, P. Fay, D. Jena, and H. Xing, IEEE Electron Device Lett. **31**(12), 1383–1385 (2010).

[4]R. Wang, G. Li, J. Verma, B. Sensale, T. Fang, J. Guo, Z. T. Hu, O. Laboutin, Y. Cao, W. Johnson, G. Snider, P. Fay, D. Jena, and H. Xing, IEEE Electron Device Lett. **32**(9), 1215–1217 (2011).

[5]R. Wang, P. Saunier, Y. Tang, T. Fang, X. Gao, S. Guo, G. Snider, P. Fay, D. Jena, and H. Xing, IEEE Electron Device Lett. **32**(3), 309–311 (2011).

[6]S. Dasgupta, Nidhi, D. Brown, F. Wu, S. Keller, J. Speck, and U. K. Mishra, Appl. Phys. Lett. **96**, 143504 (2010).

[7]K. Shinohara, A. Corrion, D. Regan, I. Milosavljevic, D. Brown, S. Burnham, P. J. Willadsen, C. Butler, A. Schmitz, D. Wheeler, A. Fung, and M. Micovic, *IEDM Tech. Dig.*, Dec. 2010, pp. 672–675.

[8]M. E. Lin, Z. Ma, F. Y. Huang, Z. F. Fan, L. H. Allen, and H. Morkoc, Appl. Phys. Lett. **64**, 1003 (1994).

[9]L. Wang, F. M. Mohammed, and I. Adesida, J. Appl. Phys. **101**, 013702 (2007).

[10]S. Ruvimov, Z. LilientalWeber, J. Washburn, K. J. Duxstad, and E. E. Haller Appl. Phys. Lett. **69**, 1556 (1996).

[11]Z. F. Fan, S. N. Mohammad, W. Kim, O. Aktas, A. E. Botchkarev, and H. Morkoc, Appl. Phys. Lett. **68**, 1672 (1996).

[12]R. E. Honig and D. A. Kramer, RCA Rev. **30**, 285 (1969).

[13]J. P. Ao, T. Wang, D. Kikuta, Y. H. Liu, S. Sakai, and Y. Ohno, Jpn. J. Appl. Phys. **42**, 1588 (2003), Part 1.

[14]D. F. Storm, D. S. Katzer, S. C. Binari, B. V. Shanabrook, L. Zhou, and D. J. Smith, Appl. Phys. Lett. **85**, 3786 (2004).

[15]C. Poblenz, P. Waltereit, S. Rajan, U. K. Mishra, J. S. Speck, P. Chin, I. Smorchkova, and B. Heying, J. Vac. Sci. Technol. B **23**, 1562 (2005).

[16]L. Zhou, D. J. Smith, D. F. Storm, D. S. Katzer, S. C. Binari, and B. V. Shanabrook, Appl. Phys. Lett. **88**, 011916 (2006).

[17]Y. Cao, T. Zimmermann, H. Xing, and D. Jena, Appl. Phys. Lett. **96**, 042102 (2010).

[18]J. G. Kim, A. C. Frenkel, H. Liu, and R. M. Park, Appl. Phys. Lett. **65**, 91 (1994).

[19]J. Guo, G. Li, F. Faria, Y. Cao, R. Wang, J. Verma, X. Gao, S. Guo, E. Beam, A. Ketterson, M. Schuette, P. Saunier, M. Wistey, D. Jena, and H. Xing, IEEE Electron Device Lett. **33**(4), 525–527 (2012).

[20]H.-J. Ueng, D. B. Janes, and K. J. Webb, IEEE Trans. Electron Devices **48**, 758–766 (2001).

[21]S. Fritze, A. Dadgar, H. Witte, M. Bügler, A. Rohrbeck, J. Bläsing, A. Hoffmann, and A. Krost, Appl. Phys. Lett. **100**, 122104 (2012).